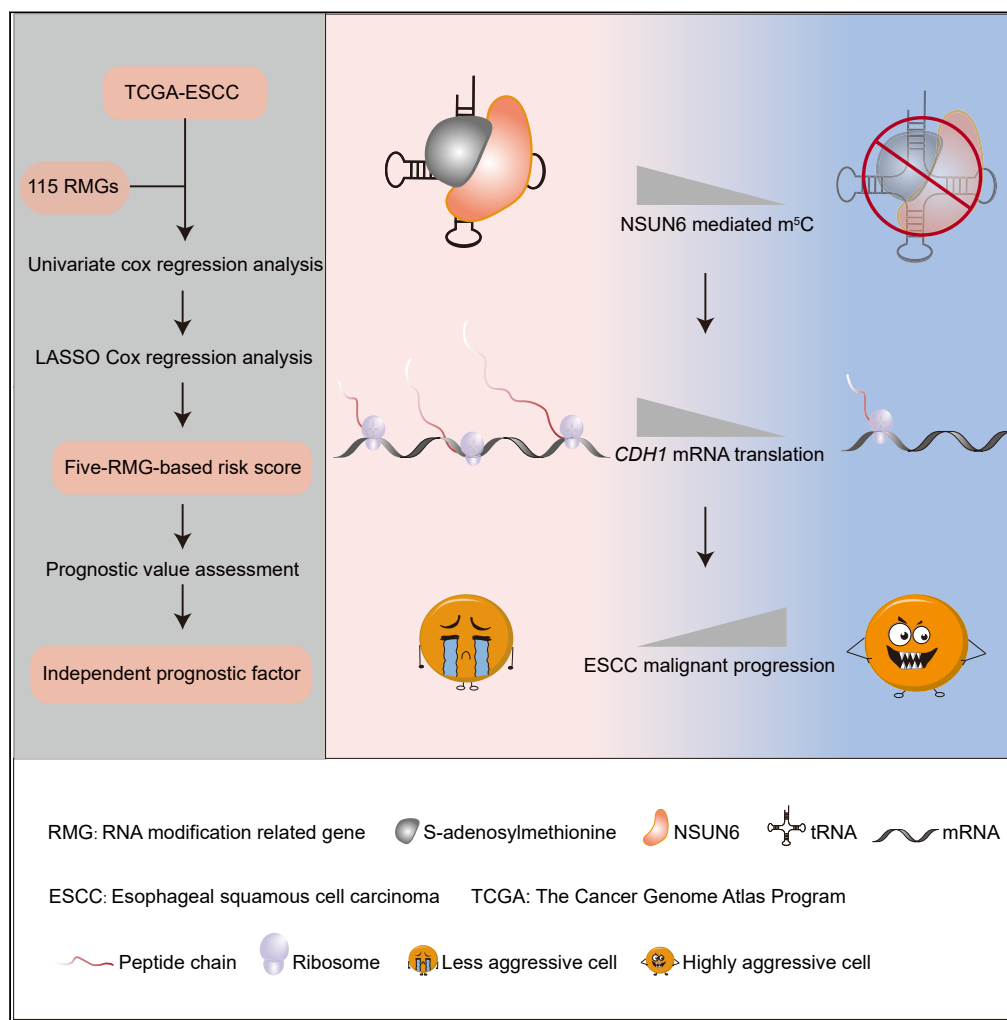


Article

# RNA modification-related genes illuminate prognostic signature and mechanism in esophageal squamous cell carcinoma



Hui Han, Yucong Sun, Wei Wei, ..., Shuibin Lin, Qianwen Liu, Shuishen Zhang

hanh23@mail2.sysu.edu.cn (H.H.)  
liuqw@sysucc.org.cn (Q.L.)  
zhangshsh9@mail.sysu.edu.cn (S.Z.)

Highlights

A five-RMG-based prognostic signature for ESCC was developed

m<sup>5</sup>C tRNA modification regulates translation efficiency in a codon-dependent manner

NSUN6 inhibits ESCC progression via modulating CDH1 mRNA translation

Han et al., iScience 27, 109327  
March 15, 2024 © 2024 The Author(s).  
<https://doi.org/10.1016/j.isci.2024.109327>



## Article

## RNA modification-related genes illuminate prognostic signature and mechanism in esophageal squamous cell carcinoma

Hui Han,<sup>1,11,\*</sup> Yucong Sun,<sup>1,11</sup> Wei Wei,<sup>2,11</sup> Zixin Huang,<sup>3,11</sup> Maosheng Cheng,<sup>1,11</sup> Hongshen Qiu,<sup>1</sup> Juan Wang,<sup>4</sup> Siyi Zheng,<sup>1</sup> Lianlian Liu,<sup>5</sup> Qiang Zhang,<sup>1</sup> Canfeng Zhang,<sup>1</sup> Jieyi Ma,<sup>1</sup> Siyao Guo,<sup>1</sup> Zhaoyu Wang,<sup>1</sup> Zhenpeng Li,<sup>6</sup> Xu Jiang,<sup>7</sup> Shuibin Lin,<sup>1</sup> Qianwen Liu,<sup>8,9,\*</sup> and Shuishen Zhang<sup>10,12,\*</sup>

## SUMMARY

Emerging studies have demonstrated the link between RNA modifications and various cancers, while the predictive value and functional mechanisms of RNA modification-related genes (RMGs) in esophageal squamous cell carcinoma (ESCC) remain unclear. Here we established a prognostic signature for ESCC based on five RMGs. The analysis of ESCC clinical samples further verified the prognostic power of the prognostic signature. Moreover, we found that the knockdown of NSUN6 promotes ESCC progression *in vitro* and *in vivo*, whereas the overexpression of NSUN6 inhibits the malignant phenotype of ESCC cells. Mechanically, NSUN6 mediated tRNA m<sup>5</sup>C modifications selectively enhance the translation efficiency of CDH1 mRNA in a codon dependent manner. Rescue assays revealed that E-cadherin is an essential downstream target that mediates NSUN6's function in the regulation of ESCC progression. These findings offer additional insights into the link between ESCC and RMGs, as well as provide potential strategies for ESCC management and therapy.

## INTRODUCTION

Esophageal cancer (ESCA) stands as one of the most lethal malignancies globally, ranking seventh in incidence and sixth in mortality across all cancer types.<sup>1,2</sup> The ailment is characterized by two histological variants: esophageal squamous cell carcinoma (ESCC) and esophageal adenocarcinoma (EAC). ESCC predominates, encompassing 85% of all esophageal cancer cases, with its highest prevalence in Asia and South Africa.<sup>3</sup> Notably, the worldwide incidence of esophageal cancer has surged dramatically, escalating over 6-fold, attributed largely to factors such as smoking and alcohol consumption.<sup>4,5</sup> Despite the emergence of treatment approaches such as multimodality neoadjuvant concurrent chemoradiotherapy (CCRT) and neoadjuvant chemoradiotherapy, the prognosis for esophageal cancer remains dismal.<sup>6,7</sup> This is largely attributed to the dearth of diagnostic tools, leading to the typical diagnosis of ESCA at advanced stages.<sup>8,9</sup> As a result, the quest for more efficacious diagnostic methodologies for patients with esophageal cancer currently takes precedence in the realm of esophageal cancer research.

RNA modifications, dynamically regulated by so-called "writers" or "erasers," are recognized and bound by "readers". "Writer" proteins introduce modifications into various RNAs and "erasers" remove them. RNA modification is a dynamic process that finely and effectively fine-tunes the activity of biological macromolecules. Over the past decade, there has been increasingly more evidence indicating a close association between RNA modification and cancers.<sup>10–14</sup> In fact, RNA modifications are increasingly being recognized as prime candidates for cancer therapy.<sup>15–17</sup> Among these, N<sup>6</sup>-methyladenosine (m<sup>6</sup>A) emerges as one of the most prevalent epitranscriptomic alterations.<sup>18–20</sup> The m<sup>6</sup>A modification, as a principal epitranscriptomic adjustment, has garnered extensive attention.<sup>21</sup> Numerous reports extensively illustrate the involvement of m<sup>6</sup>A modifications in mRNA and rRNA in orchestrating cancer progression.<sup>22</sup> Similarly, N<sup>7</sup>-methylguanosine (m<sup>7</sup>G) in tRNAs, deposited by METTL1, represents a common tRNA modification. Extensive research on m<sup>7</sup>G reveals its impact on the translation

<sup>1</sup>Center for Translational Medicine, The First Affiliated Hospital, Sun Yat-sen University, Guangzhou 510080, China

<sup>2</sup>Key Laboratory of Systems Biomedicine (Ministry of Education), Shanghai Center for Systems Biomedicine, Shanghai Jiao Tong University, Shanghai 200240, China

<sup>3</sup>Zhongshan School of Medicine, Sun Yat-sen University, Guangzhou 510080, China

<sup>4</sup>Division of Pulmonary and Critical Care Medicine, The First Affiliated Hospital, Sun Yat-sen University, Guangzhou 510080, China

<sup>5</sup>Department of Oral and Maxillofacial Surgery, The First Affiliated Hospital, Sun Yat-sen University, Guangzhou 510080, China

<sup>6</sup>Department of Microsurgery, Orthopedic Trauma and Hand Surgery, The First Affiliated Hospital, Sun Yat-sen University, Guangzhou 510080, China

<sup>7</sup>School of basic medical sciences, Southern Medical University, Guangzhou 510515, China

<sup>8</sup>Department of Thoracic Surgery, State Key Laboratory of Oncology in South China, Collaborative Innovation Center for Cancer Medicine, Sun Yat-sen University Cancer Center, Guangzhou 510080, China

<sup>9</sup>Guangdong Esophageal Cancer Institute, Guangzhou 510080, China

<sup>10</sup>Department of Thoracic Surgery, The First Affiliated Hospital, Sun Yat-sen University, Guangzhou 510080, China

<sup>11</sup>These authors contributed equally

<sup>12</sup>Lead contact

\*Correspondence: hanh23@mail2.sysu.edu.cn (H.H.), liuqw@sysucc.org.cn (Q.L.), zhangshsh9@mail.sysu.edu.cn (S.Z.)

<https://doi.org/10.1016/j.isci.2024.109327>



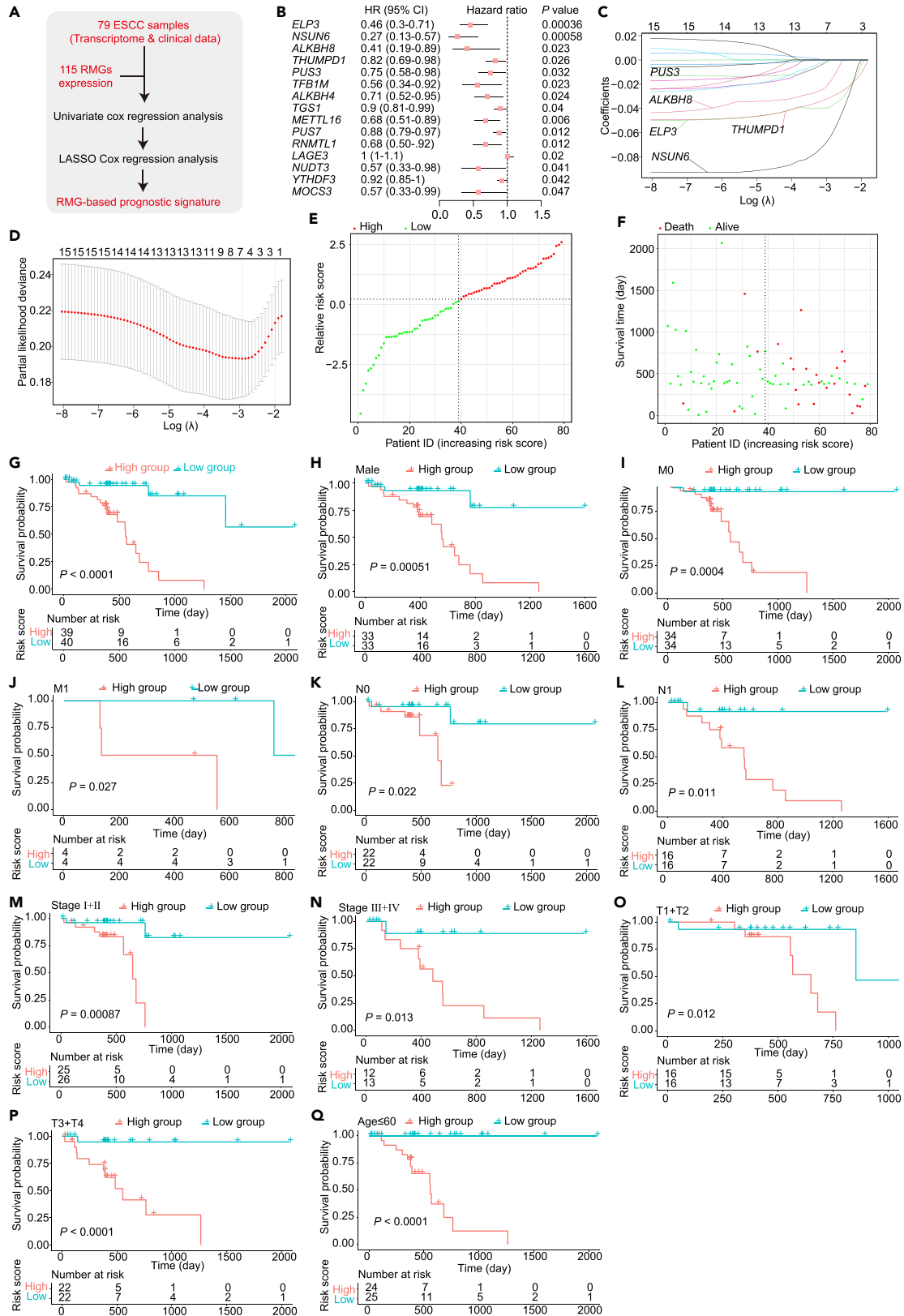


**Figure 1. Development of ESCC prognostic signature based on RNA modification-related genes**

- (A) Roadmap for assessing prognostic signature by expression levels of RMGs in patient samples.  
(B) Forest plot of hazard ratios showing the prognostic values of genes.  
(C) Coefficient spectrum of LASSO Cox regression analysis.  
(D) LASSO Cox regression analysis was employed to search for the optimal tuning parameter lambda. The horizontal axis represents log(lambda), while the vertical axis represents partial likelihood deviance. In the graph, the Lambda value corresponding to the point with the minimum partial likelihood deviance is the optimal choice. The optimal Lambda value aligns with the points below the dashed line, and the values above the dashed line indicate the optimal number of genes.  
(E) High-risk and low-risk groups are categorized according to risk scores.  
(F) Rank of prognostic index and distribution of groups.  
(G) Survival analysis of patients in high- and low-risk groups.  
(H–Q) Survival analysis of different risk score groups of patients with ESCC grouped by age, gender, TNM stages, and Grades. p values calculated by log-rank test are shown on graphs.

process, thereby exerting regulatory roles in tumor advancement.<sup>23–25</sup> These well-known modifications, such as m<sup>6</sup>A and m<sup>7</sup>G, have been extensively studied for their regulatory functions and molecular mechanisms in cancers. In recent years, 5-methylcytosine (m<sup>5</sup>C), as one of the most prominent and evolutionarily conserved RNA modifications deposited in tRNAs, rRNAs, and mRNAs, has also been increasingly associated with cancers.<sup>26,27</sup> In humans, seven members of the RNA m<sup>5</sup>C enzyme family have been identified and designated as NSUN1 to NSUN7. The biological functions of these NSUN members have undergone comprehensive investigation, revealing their pivotal roles in protein biosynthesis, cell proliferation, differentiation, and organ development. Concurrently, mutations or abnormal expressions in several NSUN members have been closely associated with various diseases. Notably, NSUN2 mutations are causative factors in autosomal recessive non-syndromic mental retardation;<sup>28</sup> NSUN5 is among the genes entirely deleted in Williams-Beuren syndrome;<sup>29</sup> NSUN3 mutations contribute to mitochondrial diseases;<sup>30</sup> NSUN7 mutations are linked to male infertility in both mice and humans,<sup>31,32</sup> and elevated the gene expression of NSUN1 and NSUN2 has been observed in various cancers.<sup>33,34</sup> NSUN6 has been reported to play a significant role in bone metastasis through the methylation of Hippo/MST1, resulting in the activation of YAP. This suggests that NSUN6 holds promise as a valuable therapeutic target for bone metastasis and therapy-resistant tumors.<sup>35</sup>

Given the crucial role of RNA modifications in cancer, the repertoire of potential targets for tumor prognosis and treatment associated with RNA modifications continues to expand. There is still substantial potential in exploring RNA modifications, such as m<sup>5</sup>C-related genes, as markers for tumor diagnosis or prognosis. Our current study endeavors to establish and validate an ESCC prognostic signature founded upon RNA modification-related genes, while also elucidating the intricate underlying mechanisms.

**RESULTS****Development of esophageal squamous cell carcinoma prognostic signature based on RNA modification-related genes**

Firstly, a list of 115 RNA modification-related genes (RMGs, Table S1) was downloaded from Modomics (<https://iimcb.genesilico.pl/modomics/>), a database of RNA modifications. Only genes in homo sapiens were included in this study. Then, we subjected the expression values of the 115 RMGs to univariate Cox regression analysis to scrutinize their correlation with overall survival (OS) probability in 79 patients with ESCC (Table S2) with comprehensive clinical attributes sourced from TCGA (Figure 1A). The findings underscored 15 genes that exhibited significant associations with OS in patients with ESCC, implying their potential relevance to patient prognosis (Figure 1B).

To refine the selection of these genes, a least absolute shrinkage and selection operator (LASSO) Cox regression analysis was executed on the identified 15 RMGs. Through this process, we identified the five most promising genes (*ELP3*, *NSUN6*, *PUS3*, *ALKBH8*, and *THUMPD1*), determined based on the  $\lambda$ -values corresponding to distinct gene counts (Figures 1C and 1D). Subsequently, a predictive risk score model for OS in patients with ESCC was developed based on the regression coefficients weighted expressions of the identified five RMGs (*ELP3*, *NSUN6*, *PUS3*, *ALKBH8*, and *THUMPD1*). The coefficients of *ELP3*, *NSUN6*, *PUS3*, *ALKBH8*, and *THUMPD1* were -0.5032, -0.8424, -0.3364, -0.0986, -0.052, respectively. Thus, the risk score for each ESCC patient was calculated with the following formula: risk score = -0.5032 × express value of *ELP3* -0.8424 × express value of *NSUN6* -0.3364 × express value of *PUS3* -0.0986 × express value of *ALKBH8* -0.052 × express value of *THUMPD1*. The 79 ESCC samples within the TCGA cohort were assigned a risk score according to the model and categorized into low- and high-risk groups using the median risk score as the threshold (Figure 1E). To validate the prognostic signature's accuracy, we compared the patient survival between the two groups. The outcomes demonstrated a significantly higher number of deaths in the high-risk group, and the OS of the low-risk group was notably superior to that of the high-risk group (Figures 1F and 1G).

Subsequently, we delved deeper into the clinical implications of the risk model. We segregated patients into two subgroups based on gender (Male, Female), M Stage (M0, M1), N Stage (N0, N1), Stage (Stage I+II, Stage III+IV), Grade (T1+T2, T3+T4), and age ( $\leq 60$ ,  $>60$ ). This exploration unveiled that the high-risk group displayed an adverse correlation with prognosis among patients aged  $\leq 60$ , males, those at differing TNM stages, or with varying Grades (Figures 1H–1Q).

**The esophageal squamous cell carcinoma prognostic model performed well as an independent prognostic indicator**

Time-dependent ROC curve was employed to assess the specificity and sensitivity of prognostic signatures. In our evaluation, the area under the curve (AUC) was determined to be 0.7564, 0.8913, and 0.8751 at 1, 2, and 3 years respectively, signifying the robust predictive performance of the model we developed (Figure 2A).

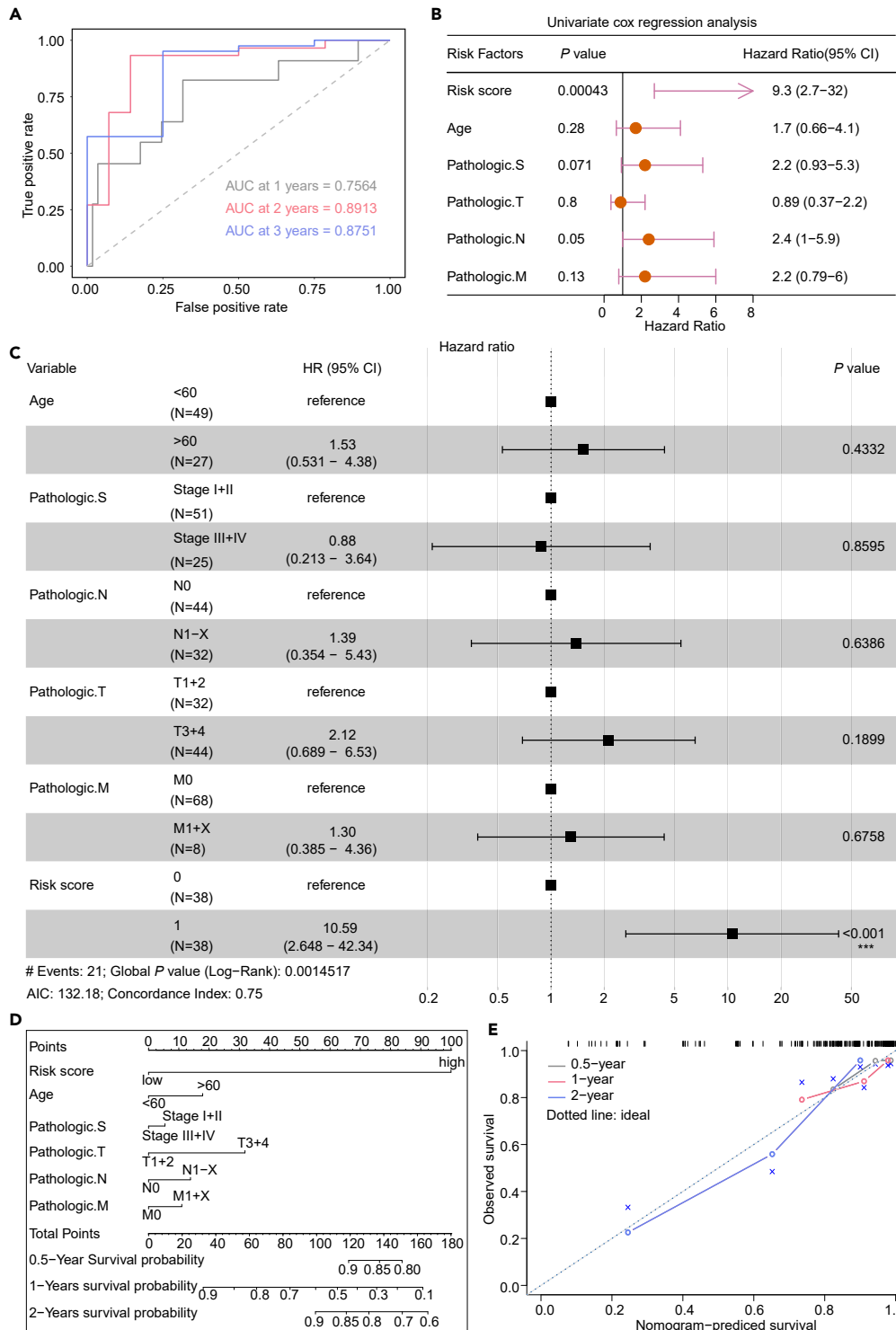


**Figure 2. The predictive efficacy of the risk model for forecasting patient prognosis**

(A) Receiver operating characteristic (ROC) curve analysis of the prognostic model in ESCC based on the survival status at 1, 2, and 3 years.

(B) Univariate Cox regression analysis of the correlation between clinical and pathological factors (including risk scores) and the overall survival rate.

(C) Multivariate Cox regression analysis of the relationship between clinical and pathological factors (including risk scores) and the overall survival rate.

(D) Nomogram constructed based on risk score, age, and stages.

(E) Calibration plot within the column chart for internal validation. The Y axis represents the actual survival rate, and the X axis represents the predicted survival rate from the nomogram.

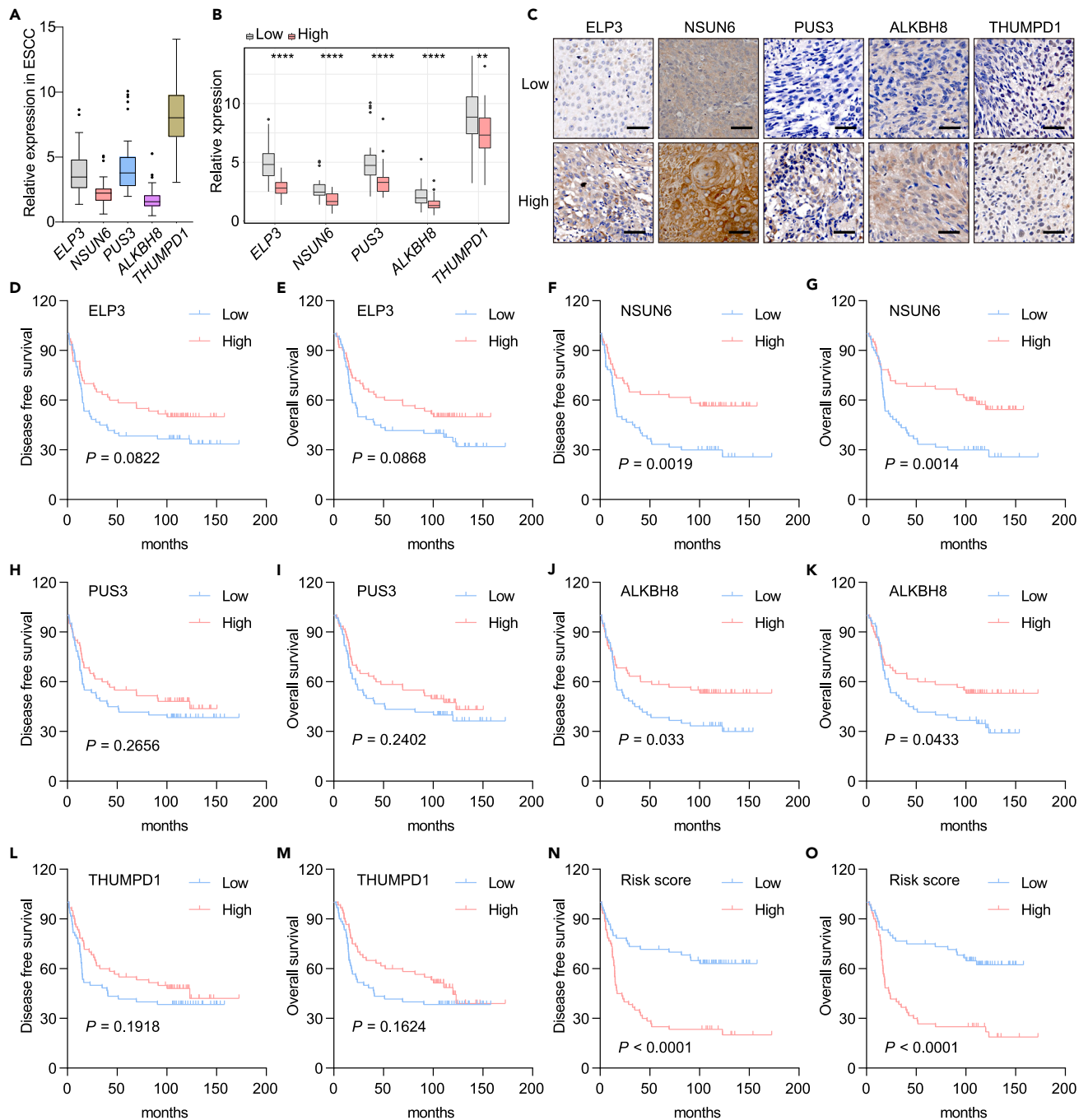


**Figure 3. Validation of the risk model using ESCC tissues**

- (A) Expression levels of the 5 RMGs in TCGA-ESCC samples.  
 (B) Expression levels of the 5 RMGs in low-risk and high-risk groups.  
 (C) Representative images of IHC staining of the 5 RMGs. Scale bar, 50  $\mu$ m.  
 (D) Disease-free survival analysis of patients with ESCC with high or low expression of ELP3.  
 (E) Overall survival analysis of patients with ESCC with high or low expression of ELP3.  
 (F) Disease-free survival analysis of patients with ESCC with high or low expression of NSUN6.  
 (G) Overall survival analysis of patients with ESCC with high or low expression of NSUN6.  
 (H) Disease-free survival analysis of patients with ESCC with high or low expression of PUS3.  
 (I) Overall survival analysis of patients with ESCC with high or low expression of PUS3.  
 (J) Disease-free survival analysis of patients with ESCC with high or low expression of ALKBH8.

**Figure 3. Continued**

(K) Overall survival analysis of patients with ESCC with high or low expression of ALKBH8.

(L) Disease-free survival analysis of patients with ESCC with high or low expression of THUMPD1.

(M) Overall survival analysis of patients with ESCC with high or low expression of THUMPD1.

(N) Disease-free survival analysis of patients with ESCC in high-risk and low-risk groups.

(O) Overall survival analysis of patients with ESCC in high-risk and low-risk groups. p values calculated by two-tailed unpaired Student's t test and log-rank test are shown on graphs. \*\* =  $p < 0.01$ , \*\*\*\* =  $p < 0.0001$ .

To further assess the viability of our risk model as an independent prognostic indicator for patients with ESCC, we initiated univariate Cox regression analyses encompassing patient age, TNM Stage, Grade, and risk score. The outcomes of these analyses indicated that the risk score (HR = 9.3, 95%CI 2.7–32,  $p < 0.001$ ) holds potential as an independent prognostic indicator for patients with ESCC (Figure 2B). Including these factors into the multivariate Cox regression, the risk score (HR = 10.59, 95%CI 2.648–42.34,  $p < 0.001$ ) remained significantly associated with the OS (Figure 2C).

All the results suggest that the prognostic signature based on these five RMGs is powerful for prognostic in patients with ESCC. The risk score can be used as an independent prognostic factor for ESCC.

**Nomogram model predicts overall survival in patients with esophageal squamous cell carcinoma**

A nomogram model was formulated incorporating six independent prognostic factors, comprising age, risk score, and TNM Stages (Figure 2D). For each ESCC sample within the TCGA dataset, vertical lines were drawn upwards from each factor to determine the corresponding points on the nomogram. The summation of these points was marked on the "total points" axis. Subsequently, a line was drawn from the total points axis to the axis representing the predicted probability of OS for patients with ESCC at 0.5, 1, and 2 years (Figure 2E). The results revealed that the calibration curve closely approximates the ideal curve in the calibration graph (represented by the dashed line), signifying the congruence between predicted OS probabilities and actual outcomes. This underscores the efficacy of the nomogram model in effectively prognosticating the OS of patients with ESCC.

**Risk score was significantly associated with RNA processing and DNA activation**

To further delve into the transcriptome characteristics of patients within the high-risk and low-risk groups, we identified genes that were differentially expressed between these two groups (Figure S1A). Gene ontology enrichment analysis revealed that these differentially expressed genes are notably enriched in processes associated with RNA processing and DNA activation (Figure S1B).

**Experimental validation of the prognostic signature**

We assessed the expression of the five candidate genes in ESCC tissues (Figure 3A) and compared their expression between the high-risk and low-risk groups in the TCGA database (Figure 3B). All five genes showed significantly higher expression levels in the low-risk group (Figure 3B), suggesting a potential negative association between their expression and the malignant progression of ESCC. However, only THUMPD1 exhibited differential expression between normal and ESCC tissues (Figures S2A–S2E).

Subsequently, we analyzed the expression of these five genes in our cohort of 120 ESCC samples from the Sun Yat-Sen University Cancer Center (Guangzhou, China) using immunohistochemical (IHC) staining. The protein levels were quantified as H-scores based on staining intensity and the proportion of cells with positive staining. The 120 ESCC samples were then categorized into low and high expression groups using the median H-score as a threshold (Figure 3C). We further investigated the correlation between the expression of these genes and the prognosis of patients with ESCC. Survival analysis revealed that the low expression of NSUN6 or ALKBH8 was associated with poor overall survival and disease-free survival, while no significant associations were observed for the other genes (Figures 3D–3M).

Obtaining mRNA expression levels for all samples was challenging. As an alternative, we calculated risk scores by applying regression coefficients to the H-scores. The top 60 individuals with the highest risk scores were classified as the high-risk group, while the remaining patients were placed in the low-risk group. Survival analysis demonstrated that patients in the high-risk group had a poorer disease-free survival (Figure 3N) and overall survival (Figure 3O), validating the robustness of the risk model established using the TCGA database.

**NSUN6 knockdown enhances esophageal squamous cell carcinoma progression *in vitro***

Next, we evaluated the expression level (Figure 4A) and perturbation effect (Figure 4B) of the five genes in ESCC cell lines using the DepMap portal (<https://depmap.org/portal/>). Among the five genes, only NSUN6 showed a negative association with the survival of ESCC cell lines (Figure 4B), which aligns with the lower expression level observed in the high-risk group. Additionally, considering that the low expression of NSUN6 is associated with poor prognosis in patients with ESCC, we speculate that NSUN6 may serve as a negative regulator of ESCC progression. NSUN6, as a methyltransferase mediates m<sup>5</sup>C modification in RNAs, was previously reported to suppress pancreatic cancer development by regulating cell proliferation.<sup>36–38</sup> We then investigate whether NSUN6 also has an inhibitory effect on the occurrence and development of ESCC. Firstly, we compared the expression of NSUN6 in ESCC cell lines (ECA109, KYSE30, and KYSE150) and normal esophageal cell line (HEEC). Our western blotting results indicate that there is a similar expression level among the three ESCC cell lines, and all these ESCC cell lines exhibit lower expression levels compared to HEEC cells (Figure 4C). Then, we executed NSUN6 knockdown (shNSUN6-1, shNSUN6-2) in two ESCC cell lines, KYSE30 (K30) and KYSE150 (K150). The reduced expression of NSUN6 was confirmed through western

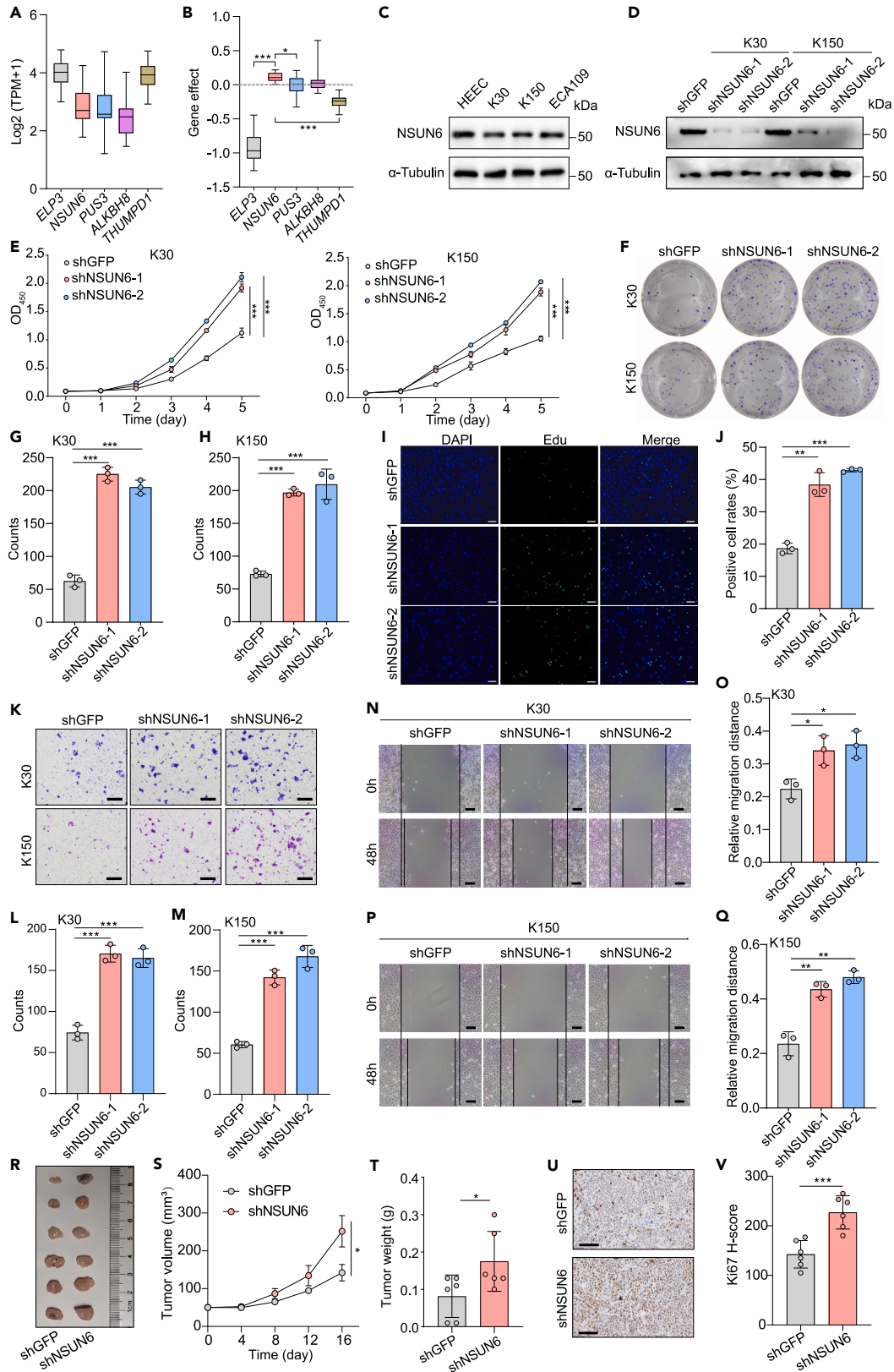


**Figure 4. Knockdown of NSUN6 promotes ESCC progression *in vitro* and *in vivo***

(A and B) Evaluation of the expression and perturbation effects of the five RMGs in ESCC cell lines using the Dependency Map (DepMap) portal.  
 (C) NSUN6 levels were detected by western blotting in HEEC, K30, K150, and ECA109 cell lines.  
 (D) Western blotting assay to detect the knockdown efficiency of NSUN6 in K150 and K30.  
 (E) CCK8 assay of cell proliferation in shNSUN6 and control ESCC cells.  
 (F–H) Representative images and quantitative analysis of colony-formation in shNSUN6 and control ESCC cells.  
 (I and J) Representative images and quantitative analysis of EdU cell proliferation assays in shNSUN6 and control ESCC cells. Scale bar, 200  $\mu$ m.  
 (K–M) Representative images and quantitative analysis of transwell invasion in shNSUN6 and control ESCC cells. Scale bar, 200  $\mu$ m.  
 (N–O) Representative images and quantitative analysis of wound healing in shNSUN6 and control ESCC cells. Scale bar, 200  $\mu$ m.  
 (R) Representative images of tumors of shNSUN6 and control groups in the xenograft mouse model.  
 (S) Volume growth curves of the tumors in the xenograft mouse model.  
 (T) Weights of the tumors in the xenograft mouse model.  
 (U and V) IHC staining for Ki67 and H-score statistics for tumors in the xenograft mouse model. Scale bar, 100  $\mu$ m. Quantitative data are shown as the mean  $\pm$  SD. p values calculated by one-way ANOVA with Dunnett's multiple comparison test and two-tailed unpaired Student's t test are shown on graphs. \* =  $p < 0.05$ , \*\* =  $p < 0.01$ , \*\*\* =  $p < 0.001$ .

blotting (Figure 4D). As expected, the CCK8 proliferation assay disclosed that NSUN6 knockdown markedly accelerated cell proliferation (Figure 4E). Correspondingly, colony-formation assays and EdU cell proliferation assays exhibited heightened ESCC cell proliferation following NSUN6 knockdown (Figures 4F–4J). The results from wound healing and transwell invasion assays indicated that the absence of NSUN6 escalated the migratory and invasive capabilities of ESCC cells (Figures 4K–4Q).

**NSUN6 knockdown enhances esophageal squamous cell carcinoma progression *in vivo***

To gain insights into the *in vivo* impact of NSUN6, we conducted subcutaneous injections of control or shNSUN6 ESCC cells into nude mice employing a xenograft mouse model. The results underscored that NSUN6 knockdown augmented the tumorigenic potential of ESCC *in vivo* (Figures 4R–4T). Immunohistochemical staining of Ki67 demonstrated that NSUN6 knockdown promotes ESCC cell growth *in vivo* (Figures 4U and 4V). Consequently, we concluded that NSUN6 knockdown augments the functional attributes of ESCC cells both *in vitro* and *in vivo*.

**Overexpression of NSUN6 suppresses esophageal squamous cell carcinoma progression**

To further ascertain the role of NSUN6 in ESCC, we proceeded to overexpress NSUN6 (oeNSUN6) in K30 and K150 cells. Western blotting was performed to confirm the overexpression of NSUN6 (Figure 5A). CCK8 and colony-formation assays underscored that the overexpression of NSUN6 curbed the proliferation capability of ESCC cells (Figures 5B–5D). Transwell invasion assay revealed that ESCC cell invasive potential was decelerated in the overexpression of NSUN6, as opposed to the control group (Figures 5E and 5F). Similarly, elevated NSUN6 levels hindered the migration ability of ESCC cells, as confirmed by the wound healing assays (Figures 5G and 5H). In summary, augmenting NSUN6 expression led to the inhibition of ESCC progression *in vitro*.

**NSUN6 regulates 5-methylcytosine tRNA modification and mRNA translation in esophageal squamous cell carcinoma**

Previous studies have demonstrated that NSUN6, as a m<sup>5</sup>C methyltransferase, is mainly responsible for m<sup>5</sup>C deposited in tRNA<sup>Cys</sup> and tRNA<sup>Thr</sup> and regulates mRNA translation.<sup>39–41</sup> Some studies reported that NSUN6 also catalyzes m<sup>5</sup>C modification in mRNAs.<sup>38,42</sup> To study the molecular mechanisms underlying NSUN6's function in ESCC progression, we conducted mass spectrometry analysis to detect m<sup>5</sup>C modification levels in total RNAs and purified tRNAs in NSUN6 knockdown or control ESCC cells (Figure 6A). The results demonstrated that global m<sup>5</sup>C levels were merely changed, while m<sup>5</sup>C levels in tRNAs were significantly decreased upon NSUN6 knockdown (Figures 6B–6G), suggesting that NSUN6 mainly responsible for tRNA m<sup>5</sup>C modification in ESCC cells.

Given that tRNAs function in mRNA translation, we next determined the effect of NSUN6 on mRNA translation in ESCC cells. In our puromycin intake assay, a 20% reduction in cellular protein synthesis rates following NSUN6 knockdown was observed (Figures 6H and 6I).

**NSUN6 selectively regulates mRNA translation in a codon dependent manner**

To study the effect of translation disorder mediated by abnormal m<sup>5</sup>C tRNA modification, we performed ribosome-nascent chain complex-bound mRNA sequencing (RNC-seq) to profile mRNA translation efficiencies in shNSUN6 and control ESCC cells (Figure 6J). We identified 1683 down-regulated genes and 649 up-regulated genes out of 17065 detected genes based on their translation efficiencies (TEs) in the shNSUN6 cells compared to control ESCC cells (Figure 6K). To investigate the link between the mRNA translation and tRNA m<sup>5</sup>C modification, we calculated the number of the codons (ACA, ACC, ACG, ACT, TGC, and TGT) decoded by tRNA<sup>Cys</sup> and tRNA<sup>Thr</sup>, the substrates of NSUN6, on differentially translated mRNAs. Our data revealed that the mRNAs with reduced TE have a notably larger number of codons decoded by tRNA<sup>Cys</sup> and tRNA<sup>Thr</sup> (Figures 6L and 6M), suggesting that NSUN6 selectively regulates mRNA translation in a codon dependent manner.

Through pathway enrichment and molecular function enrichment analyses, we highlighted a significant enrichment of TE down-regulated genes. The E-cadherin-related pathway emerged prominently in both modes of enrichment, indicating a tight correlation between E-cadherin-related pathway and NSUN6 (Figures 6N–6P). Notably, under the selective regulation of mRNA translation mechanism, several crucial signaling

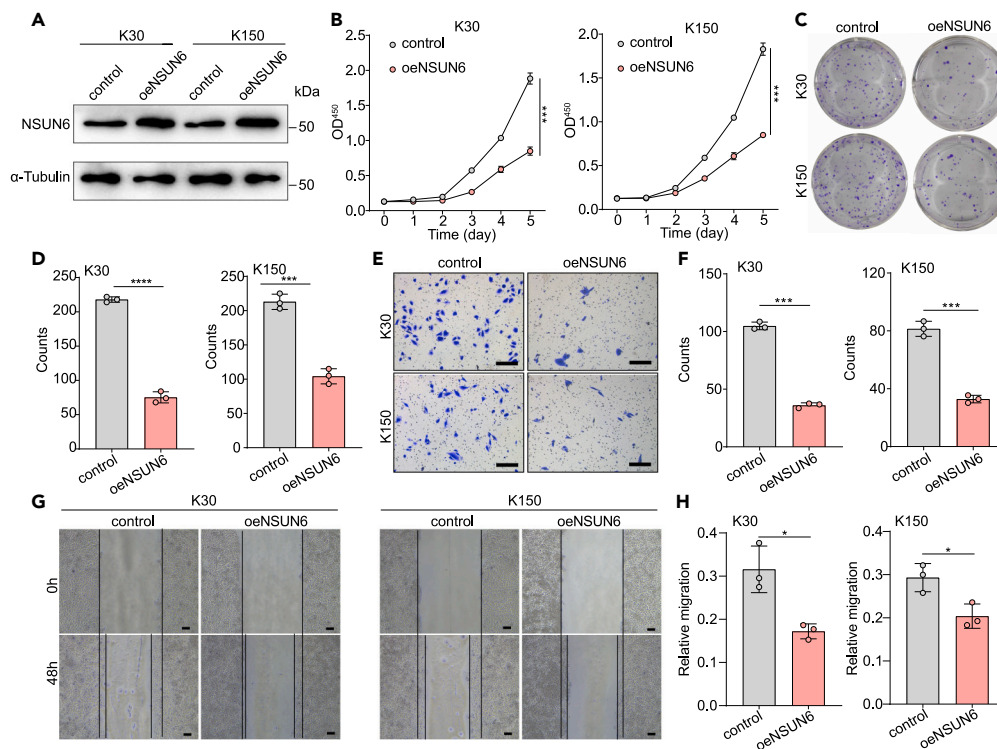


**Figure 5. Overexpression of NSUN6 inhibits ESCC progression**

(A) Western blotting assay to detect the overexpression efficiency of NSUN6 in K150 and K30.

(B) CCK8 assay of oeNSUN6 and control ESCC cells.

(C and D) Representative images and quantitative analysis of colony-formation in oeNSUN6 and control ESCC cells.

(E and F) Representative images and quantitative analysis of transwell invasion in oeNSUN6 and control ESCC cells. Scale bar, 200  $\mu$ m.

(G and H) Representative images and quantitative analysis of wound healing in shNSUN6 and control ESCC cells. Scale bar, 200  $\mu$ m. Quantitative data are shown as the mean  $\pm$  SD. p values calculated by two-tailed unpaired Student's t test are shown on graphs. \* = p < 0.05, \*\* = p < 0.01, \*\*\* = p < 0.001.

pathways typically associated with cancer promotion including the EGFR signaling pathway, mTOR signaling pathway, PI3K signaling pathway, NOTCH signaling pathway, and MAPK signaling pathway, remained unaffected by NSUN6 knockdown (Figures S3A–S3E).

Homophilic binding of E-cadherin between cells plays a crucial role in facilitating the contact inhibition of proliferation when cells attain confluence.<sup>43</sup> The diminishment of E-cadherin expression leads to the forfeiture of contact inhibition, coupled with heightened cell motility and progression to advanced cancer stages. Hence, we posited that NSUN6 impacts the progression of ESCC by modulating the mRNA translation of E-cadherin. To verify this hypothesis, real-time quantitative PCR (qRT-PCR) assays using the input-mRNA or RNC-mRNAs isolated from K150 cells with or without NSUN6 knockdown were performed and the results demonstrated that the depletion of NSUN6 leads to a significant reduction of *CDH1* (gene encoding E-cadherin protein) translation efficiency, while do not impair the mRNA level of *CDH1* (Figures 6Q and 6R). Furthermore, immunofluorescence assay of tumors from the xenograft mouse model displayed a significant reduction in E-cadherin levels upon NSUN6 knockdown in the subcutaneous tumor, indicating a more malignant phenotype (Figure 6S). In addition, western blotting was performed and the results showed a significant decrease in the E-cadherin protein level upon NSUN6 knockdown (Figure S4). Notably, the regulation of *CDH1* mRNA translation by NSUN6 is not attributed to m<sup>5</sup>C modifications on *CDH1* itself. In fact, the previous methylation profiling by high throughput sequencing (GSE148764) did not identify *CDH1* as a substrate of NSUN6.<sup>42</sup>

### E-cadherin is a key downstream target of NSUN6 in esophageal squamous cell carcinoma

To verify the role of E-cadherin in NSUN6's function in ESCC, we performed a rescue assay to re-introduce E-cadherin into NSUN6 knockdown ESCC cells (Figure 7A). CCK8 and colony-formation assays underscored that the re-expression of NSUN6 mitigated the increased proliferation capability of ESCC cells (Figures 7B–7D). Transwell invasion assay revealed that ESCC cell invasive potential was decelerated in the overexpression of E-cadherin, as opposed to the shNSUN6 group (Figures 7E and 7F). Similarly, elevated E-cadherin levels hindered the migration ability of NSUN6 knockdown ESCC cells, as confirmed by the wound healing assays (Figures 7G and 7H). Overall, these data revealed that E-cadherin is a key downstream target of NSUN6 and further supported that NSUN6 mediated tRNA m<sup>5</sup>C modification represses ESCC progression through the regulation of E-cadherin.

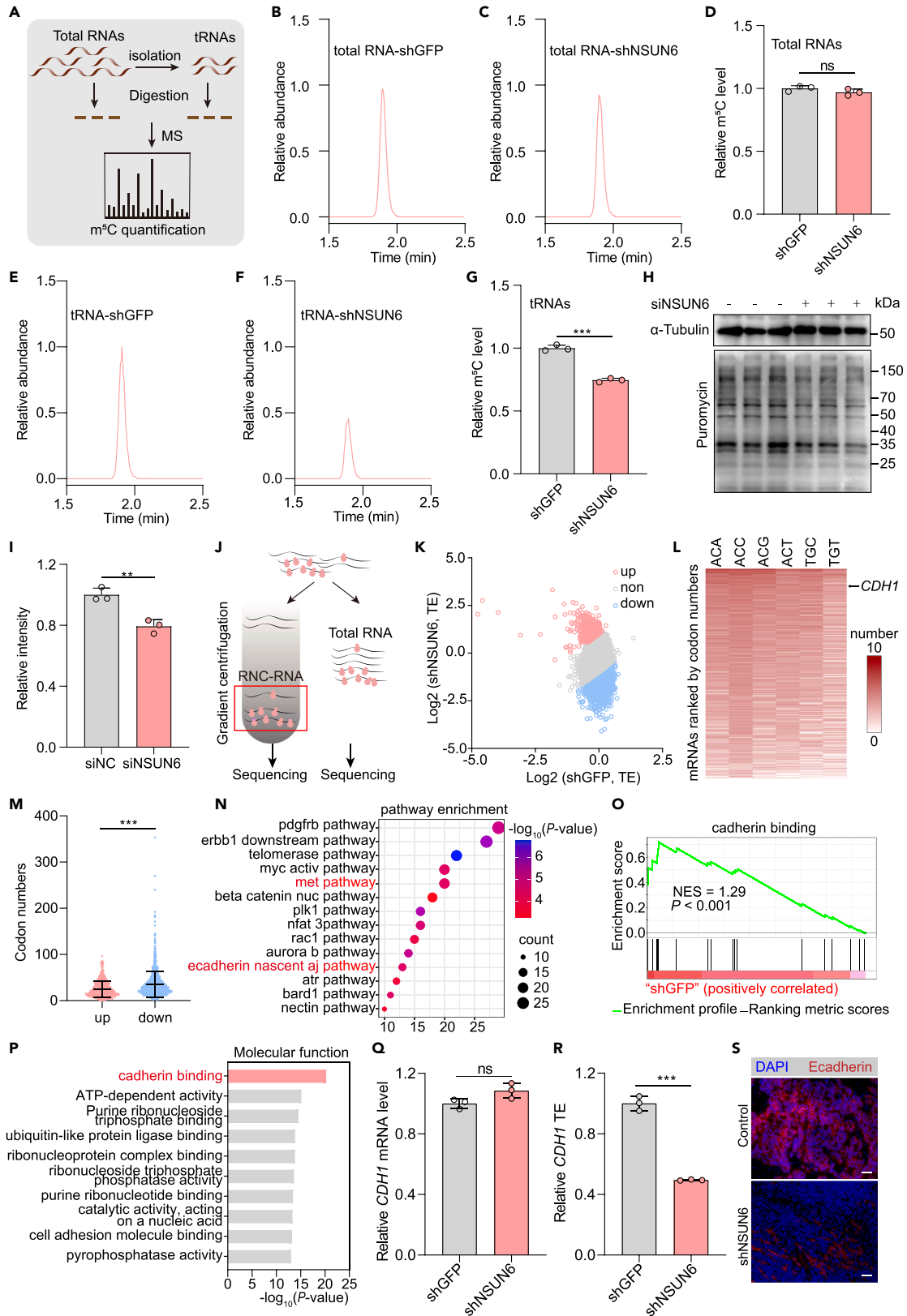


**Figure 6. NSUN6-mediated m<sup>5</sup>C tRNA modification selectively regulates CDH1 mRNA translation in a codon dependent manner**

- (A) Schematic diagram for measuring m<sup>5</sup>C abundance in total RNAs and tRNAs in ESCC cells.  
(B–D) Mass spectrometry measurements of the m<sup>5</sup>C abundance of total RNAs in shNSUN6 and control ESCC cells.  
(E–G) Mass spectrometry measurements of the m<sup>5</sup>C abundance of tRNAs in shNSUN6 and control ESCC cells.  
(H and I) Puromycin intake assay of ESCC cells with or without NSUN6 knockdown.  
(J) The principle and workflow diagram of RNC-seq, where pink units represent ribosomes.  
(K) The mRNAs sequenced by RNC-seq are classified based on their TE values. Pink denotes genes with upregulated TE after NSUN6 knockdown, gray represents genes with little changes in TE post NSUN6 knockdown, while blue signifies genes with downregulated TE after NSUN6 knockdown.  
(L) Heatmap of codons decoded by tRNA<sup>Cys</sup> and tRNA<sup>Thr</sup> within mRNA detected in RNC-seq.  
(M) Number of codons decoded by tRNA<sup>Cys</sup> and tRNA<sup>Thr</sup> on TE down- and up-regulated mRNAs.  
(N–P) Pathway enrichment analysis and molecular function analysis using the TE-down genes.  
(Q) *CDH1* mRNA levels in shNSUN6 and control ESCC cells.  
(R) TE of *CDH1* in shNSUN6 and control ESCC cells.  
(S) Representative images of immunofluorescence staining of E-cadherin in shNSUN6 and control ESCC cells. Scale bar, 50 μm. Quantitative data are shown as mean ± SD from three independent experiments. p values calculated by two-tailed unpaired Student's t test are shown on graphs. ns = p > 0.05, \*\* = p < 0.01, \*\*\* = p < 0.001.

**DISCUSSION**

Over 150 RNA modifications have been identified, encompassing diverse types such as m<sup>5</sup>C, 5-hydroxymethylcytosine (hm<sup>5</sup>C), N1-methyladenine (m<sup>1</sup>A), m<sup>7</sup>G, N6,2'-O-dimethyladenosine (m<sup>6</sup>A.m.), N4-acetylcytidine (ac4C), and more. Notably, methylation modification takes precedence as the most abundant endogenous RNA modification in eukaryotes, constituting over 50% of all RNA modifications.<sup>44,45</sup> RNA methylation, along with its downstream signaling pathways, assumes a pivotal role in an array of biological processes. These encompass cell differentiation, sex determination, and stress response, among others.<sup>46–49</sup> Due to their intimate connection with cancer, RNA methylations are poised to emerge as innovative indicators for cancer diagnosis. Their intricate relationship with cancer processes implies their potential to serve as diagnostic markers.<sup>50,51</sup>

To unravel the intricate relationship between RNA modification and the prognosis of patients with ESCC, our investigation commenced with a detailed analysis of gene expression patterns in a cohort of 79 patients with ESCC in TCGA. Our study revealed a robust prognostic signature for ESCC rooted in the complex landscape of RMGs. The established five-RMG-based prognostic signature, rigorously validated using both the TCGA-ESCC database and clinical samples, emerges as a promising, independent, and reliable indicator of ESCC prognosis. These findings suggest a promising avenue in exploring RMGs as potential diagnostic markers for various cancers, including ESCC. The highlighted aberrant expression patterns of RMGs in cancer underscore the potential utility of specific RNA modifications as non-invasive biomarkers for cancer diagnosis. Future investigations could concentrate on the development of sensitive and specific assays capable of detecting these modifications in biofluids, offering a minimally invasive approach for early cancer detection and continuous monitoring. This holistic approach aligns with the broader goal of advancing precision medicine in cancer diagnosis and prognosis.

The identified NSUN6, emerged as pivotal players in modulating ESCC progression. Knockdown experiments revealed a promoting effect on ESCC progression, while NSUN6 overexpression showcased an inhibitory impact on the malignant phenotype of ESCC cells. This functional duality of NSUN6 suggests its potential as a therapeutic target for ESCC management. At the molecular level, our study uncovered a mechanism by which NSUN6 regulates ESCC progression. NSUN6-mediated tRNA m<sup>5</sup>C modifications were found to selectively enhance the translation efficiency of *CDH1* mRNA in a codon-dependent manner. This mechanism provides a foundation for understanding the underlying molecular processes. The rescue assays further implicated E-cadherin as a key downstream target mediating NSUN6's regulatory function in ESCC progression. This finding connects the dots between NSUN6, tRNA modifications, and the *CDH1* mRNA translation, offering a comprehensive understanding of the molecular pathways involved in ESCC.

Despite these promising prospects, it is crucial to acknowledge the limitations of our study. While we globally assessed NSUN6-mediated m<sup>5</sup>C modifications, the lack of precise identification of NSUN6 substrate RNAs represents a gap in our understanding. Future studies employing advanced RNA sequencing techniques can provide a more detailed map of NSUN6 interactions with specific RNA molecules. Additionally, the exact mechanisms through which tRNA m<sup>5</sup>C modifications regulate mRNA translation remain elusive. A deeper investigation into the specific pathways and interactions involved in this process will provide a more comprehensive understanding of the molecular intricacies at play.

The developed prognostic signature can serve as a valuable tool for clinicians to assess patient outcomes, guiding personalized treatment strategies. Furthermore, the delineated molecular mechanisms involving NSUN6 and E-cadherin open up possibilities for targeted therapies aiming to disrupt specific pathways implicated in ESCC progression. In conclusion, our findings underscore the importance of RMGs, particularly NSUN6, in shaping the landscape of ESCC. The prognostic signature and mechanistic insights provided by this study may pave the way for the development of potential therapeutic strategies for ESCC, ultimately improving patient outcomes. Future research may delve deeper into the functional roles of other identified RMGs and explore additional layers of complexity in the RNA modification landscape of ESCC. Addressing the identified limitations and continuing to unravel the complexities of RNA modification networks will undoubtedly enhance our understanding and contribute to the development of innovative strategies for cancer management.

**Limitations of the study**

While validating the prognostic signature using clinical samples, we adopted the H-score instead of the mRNA level to calculate the risk score. This substitution may introduce some degree of error, and the use of mRNA levels could offer a more accurate assessment. The precise

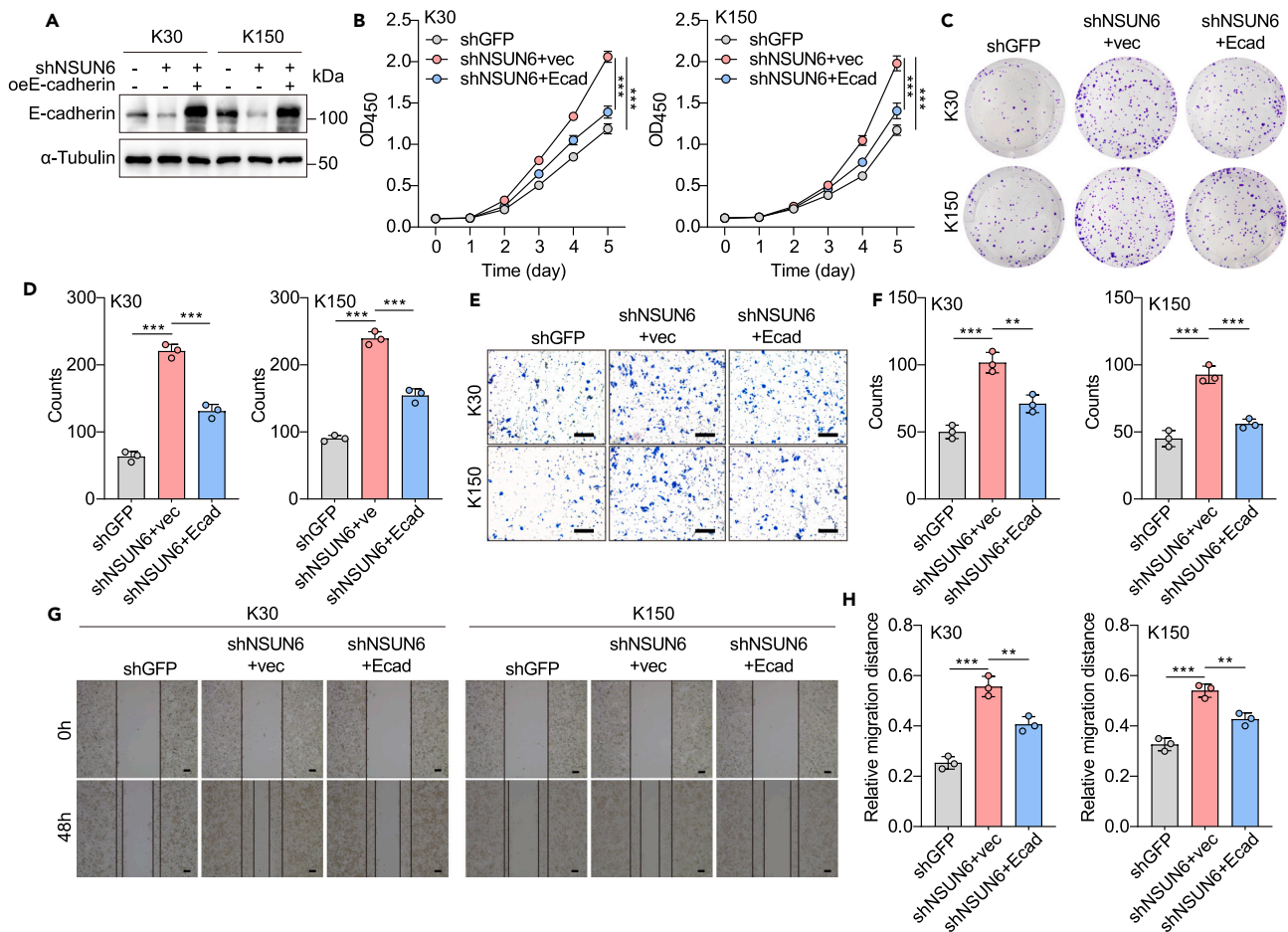


**Figure 7. E-cadherin is a key downstream target of NSUN6 in ESCC**

(A) Western blotting assay to detect the overexpression efficiency of E-cadherin in shNSUN6 ESCC cells.

(B) CCK8 assay of cell proliferation.

(C and D) Representative images and quantitative analysis of colony-formation.

(E and F) Representative images and quantitative analysis of transwell invasion. Scale bar, 200  $\mu$ m.

(G and H) Representative images and quantitative analysis of wound healing. Scale bar, 200  $\mu$ m. Quantitative data are shown as the mean  $\pm$  SD. p values calculated by one-way ANOVA with Dunnett's multiple comparison test are shown on graphs. \*\* = p < 0.01, \*\*\* = p < 0.001. vec = vector, Ecad = E-cadherin.

identification of NSUN6-mediated m<sup>5</sup>C modifications on specific RNA substrates and the details on how NSUN6-mediated m<sup>5</sup>C modifications regulate mRNA translation necessitate further investigation.

## STAR★METHODS

Detailed methods are provided in the online version of this paper and include the following:

- [KEY RESOURCES TABLE](#)
- [RESOURCE AVAILABILITY](#)
  - Lead contact
  - Materials availability
  - Data and code availability
- [EXPERIMENTAL MODEL AND STUDY PARTICIPANT DETAILS](#)
  - Patient samples
  - Xenograft mouse model
- [METHOD DETAILS](#)
  - Data retrieval and preprocessing
  - Modeling of prognostic relevance

- Construction of a predictive nomogram
- Cell culture
- Knockdown or overexpression of NSUN6 in ESCC cells
- Western blotting
- Colony-formation, cell proliferation assays
- Wound healing
- Transwell invasion
- Immunohistochemistry (IHC) staining
- RNA mass spectrometry analysis
- Ribosome-nascent chain complex-bound mRNA sequencing (RNC-seq)
- RNA isolation and qRT-PCR
- Immunofluorescence
- Gene pathway enrichment and depmap analysis
- QUANTIFICATION AND STATISTICAL ANALYSIS
- ADDITIONAL RESOURCES

### SUPPLEMENTAL INFORMATION

Supplemental information can be found online at <https://doi.org/10.1016/j.isci.2024.109327>.

### ACKNOWLEDGMENTS

This study was supported by grants from National Natural Science Foundation of China (Grant No.82103077 to S.S.Z.), Natural Science Foundation of Guangdong Province, China (2023A1515010513 to S.S.Z.), and Young Talent Support Project of Guangzhou Association for Science and Technology (QT-2023-026 to S.S.Z.). We thank Dr. Demeng Chen for his helpful comments and suggestions.

### AUTHOR CONTRIBUTIONS

S.S.Z., Q.W.L., H.H., and S.B.L. conceived and designed the study. H.H., Y.C.S., W.W., Z.X.H., and M.S.C. designed and performed the experiments. W.W., Z.X.H., and M.S.C. performed data collection. H.S.Q., J.W., L.L.L., Q.Z., S.Y.Z., C.F.Z., and J.Y.M. analyzed and interpreted the data. S.Y.G., Z.Y.W., Z.P.L., and X.J. helped with some experiments. All authors read and approved the final article.

### DECLARATION OF INTERESTS

All authors declare that they have no conflict of interests.

Received: October 2, 2023

Revised: January 6, 2024

Accepted: February 20, 2024

Published: February 24, 2024

### REFERENCES

1. Sung, H., Ferlay, J., Siegel, R.L., Laversanne, M., Soerjomataram, I., Jemal, A., and Bray, F. (2021). Global Cancer Statistics 2020: GLOBOCAN Estimates of Incidence and Mortality Worldwide for 36 Cancers in 185 Countries. *CA A Cancer J. Clin.* *71*, 209–249. <https://doi.org/10.3322/caac.21660>.
2. Juergens, R.A., and Forastiere, A. (2008). Combined modality therapy of esophageal cancer. *J. Natl. Compr. Cancer Netw.* *6*, 851–861. <https://doi.org/10.6004/jnccn.2008.0063>.
3. Smyth, E.C., Lagergren, J., Fitzgerald, R.C., Lordick, F., Shah, M.A., Lagergren, P., and Cunningham, D. (2017). Oesophageal cancer. *Nat. Rev. Dis. Prim.* *3*, 17048. <https://doi.org/10.1038/nrdp.2017.48>.
4. Huang, F.L., and Yu, S.J. (2018). Esophageal cancer: Risk factors, genetic association, and treatment. *Asian J. Surg.* *41*, 210–215. <https://doi.org/10.1016/j.asjsur.2016.10.005>.
5. Simard, E.P., Ward, E.M., Siegel, R., and Jemal, A. (2012). Cancers with increasing incidence trends in the United States: 1999 through 2008. *CA A Cancer J. Clin.* *62*, 118–128. <https://doi.org/10.3322/caac.20141>.
6. Merkow, R.P., Bilimoria, K.Y., McCarter, M.D., Chow, W.B., Ko, C.Y., and Bentrem, D.J. (2012). Use of multimodality neoadjuvant therapy for esophageal cancer in the United States: assessment of 987 hospitals. *Ann. Surg. Oncol.* *19*, 357–364. <https://doi.org/10.1245/s10434-011-1945-3>.
7. van den Ende, T., Ezdoglian, A., Baas, L.M., Bakker, J., Lougheed, S.M., Harrasser, M., Waasdorp, C., van Berge Henegouwen, M.I., Hulshof, M.C.C.M., Haj Mohammad, N., et al. (2023). Longitudinal immune monitoring of patients with resectable esophageal adenocarcinoma treated with Neoadjuvant PD-L1 checkpoint inhibition. *Oncol Immunology* *12*, 2233403. <https://doi.org/10.1080/2162402x.2023.2233403>.
8. Wei, W., Zhang, S., Han, H., Wang, X., Zheng, S., Wang, Z., Yang, C., Wang, L., Ma, J., Guo, S., et al. (2023). NAT10-mediated ac4C tRNA modification promotes EGFR mRNA translation and gefitinib resistance in cancer. *Cell Rep.* *42*, 112810. <https://doi.org/10.1016/j.celrep.2023.112810>.
9. Stahl, M., and Oliveira, J.; ESMO Guidelines Working Group (2009). Esophageal cancer: ESMO clinical recommendations for diagnosis, treatment and follow-up. *Ann. Oncol.* *20*, 32–33. <https://doi.org/10.1093/annonc/mdp121>.
10. Mun, E.J., Babiker, H.M., Weinberg, U., Kirson, E.D., and Von Hoff, D.D. (2018). Tumor-Treating Fields: A Fourth Modality in Cancer Treatment. *Clin. Cancer Res.* *24*, 266–275. <https://doi.org/10.1158/1078-0432.Ccr-17-1117>.
11. Boshuizen, J., and Peeper, D.S. (2020). Rational Cancer Treatment Combinations: An Urgent Clinical Need. *Mol. Cell* *78*, 1002–

1018. <https://doi.org/10.1016/j.molcel.2020.05.031>.
12. (2022). Cancer Diagnosis, Treatment Linked to Suicide Risk. *Cancer Discov.* 12, Of2. <https://doi.org/10.1158/2159-8290.Cd-nb2022-0032>.
  13. Han, H., Zheng, S., and Lin, S. (2023). N(7)-methylguanosine (m7G) tRNA modification: a novel autophagy modulator in cancer. *Autophagy* 19, 360–362. <https://doi.org/10.1080/15548627.2022.2077551>.
  14. Han, H., Yang, C., Zhang, S., Cheng, M., Guo, S., Zhu, Y., Ma, J., Liang, Y., Wang, L., Zheng, S., et al. (2021). METTL3-mediated m(6A) mRNA modification promotes esophageal cancer initiation and progression via Notch signaling pathway. *Mol. Ther. Nucleic Acids* 26, 333–346. <https://doi.org/10.1016/j.omtn.2021.07.007>.
  15. Barbieri, I., and Kouzarides, T. (2020). Role of RNA modifications in cancer. *Nat. Rev. Cancer* 20, 303–322. <https://doi.org/10.1038/s41568-020-0253-2>.
  16. Revia, R.A., Stephen, Z.R., and Zhang, M. (2019). Theranostic Nanoparticles for RNA-Based Cancer Treatment. *Acc. Chem. Res.* 52, 1496–1506. <https://doi.org/10.1021/acs.accounts.9b00101>.
  17. Xie, Z., and Zeng, X. (2017). DNA/RNA-based formulations for treatment of breast cancer. *Exp. Opin. Drug Deliv.* 14, 1379–1393. <https://doi.org/10.1080/17425247.2017.1317744>.
  18. Li, X., Ma, S., Deng, Y., Yi, P., and Yu, J. (2022). Targeting the RNA m(6A) modification for cancer immunotherapy. *Mol. Cancer* 21, 76. <https://doi.org/10.1186/s12943-022-01558-0>.
  19. Sun, T., Wu, R., and Ming, L. (2019). The role of m6A RNA methylation in cancer. *Biomed. Pharmacother.* 112, 108613. <https://doi.org/10.1016/j.biopha.2019.108613>.
  20. Müller, S., Glaß, M., Singh, A.K., Haase, J., Bley, N., Fuchs, T., Lederer, M., Dahl, A., Huang, H., Chen, J., et al. (2019). IGF2BP1 promotes SRF-dependent transcription in cancer in a m6A- and miRNA-dependent manner. *Nucleic Acids Res.* 47, 375–390. <https://doi.org/10.1093/nar/gky1012>.
  21. Peng, H., Chen, B., Wei, W., Guo, S., Han, H., Yang, C., Ma, J., Wang, L., Peng, S., Kuang, M., and Lin, S. (2022). N(6)-methyladenosine (m6A) in 18S rRNA promotes fatty acid metabolism and oncogenic transformation. *Nat. Metab.* 4, 1041–1054. <https://doi.org/10.1038/s42255-022-00622-9>.
  22. Lin, S., Choe, J., Du, P., Triboulet, R., and Gregory, R.I. (2016). The m(6A) Methyltransferase METTL3 Promotes Translation in Human Cancer Cells. *Mol. Cell* 62, 335–345. <https://doi.org/10.1016/j.molcel.2016.03.021>.
  23. Huang, X., Chen, Z., Xiang, X., Liu, Y., Long, X., Li, K., Qin, M., Long, C., Mo, X., Tang, W., and Liu, J. (2022). Comprehensive multi-omics analysis of the m7G in pan-cancer from the perspective of predictive, preventive, and personalized medicine. *EPMA J.* 13, 671–697. <https://doi.org/10.1007/s13167-022-00305-1>.
  24. Orellana, E.A., Liu, Q., Yankova, E., Pirouz, M., De Braekeleer, E., Zhang, W., Lim, J., Aspris, D., Sendinc, E., Gargallo, D.A., et al. (2021). METTL1-mediated m(7)G modification of Arg-TCT tRNA drives oncogenic transformation. *Mol. Cell* 81, 3323–3338.e14. <https://doi.org/10.1016/j.molcel.2021.06.031>.
  25. Li, L., Yang, Y., Wang, Z., Xu, C., Huang, J., and Li, G. (2021). Prognostic role of METTL1 in glioma. *Cancer Cell Int.* 21, 633. <https://doi.org/10.1186/s12935-021-02346-4>.
  26. Wang, Y., Wei, J., Feng, L., Li, O., Huang, L., Zhou, S., Xu, Y., An, K., Zhang, Y., Chen, R., et al. (2023). Aberrant m5C hypermethylation mediates intrinsic resistance to gefitinib through NSUN2/YBX1/QSOX1 axis in EGFR-mutant non-small-cell lung cancer. *Mol. Cancer* 22, 81. <https://doi.org/10.1186/s12943-023-01780-4>.
  27. Hu, Y., Chen, C., Tong, X., Chen, S., Hu, X., Pan, B., Sun, X., Chen, Z., Shi, X., Hu, Y., et al. (2021). NSUN2 modified by SUMO-2/3 promotes gastric cancer progression and regulates mRNA m5C methylation. *Cell Death Dis.* 12, 842. <https://doi.org/10.1038/s41419-021-04127-3>.
  28. Khan, M.A., Rafiq, M.A., Noor, A., Hussain, S., Flores, J.V., Rupp, V., Vincent, A.K., Malli, R., Ali, G., Khan, F.S., et al. (2012). Mutation in NSUN2, which encodes an RNA methyltransferase, causes autosomal-recessive intellectual disability. *Am. J. Hum. Genet.* 90, 856–863. <https://doi.org/10.1016/j.ajhg.2012.03.023>.
  29. Merla, G., Ucla, C., Guipponi, M., and Raymond, A. (2002). Identification of additional transcripts in the Williams-Beuren syndrome critical region. *Hum. Genet.* 110, 429–438. <https://doi.org/10.1007/s00439-002-0710-x>.
  30. Van Haute, L., Dietmann, S., Kremer, L., Hussain, S., Pearce, S.F., Powell, C.A., Rorbach, J., Lantaff, R., Blanco, S., Sauer, S., et al. (2016). Deficient methylation and formylation of mt-tRNA(Met) wobble cytosine in a patient carrying mutations in NSUN3. *Nat. Commun.* 7, 12039. <https://doi.org/10.1038/ncomms12039>.
  31. Harris, T., Marquez, B., Suarez, S., and Schimenti, J. (2007). Sperm motility defects and infertility in male mice with a mutation in Nsun7, a member of the Sun domain-containing family of putative RNA methyltransferases. *Biol. Reprod.* 77, 376–382. <https://doi.org/10.1095/biolreprod.106.058669>.
  32. Khosronezhad, N., Colagar, A.H., and Jorsarayi, S.G.A. (2015). T26248G-transversion mutation in exon7 of the putative methyltransferase Nsun7 gene causes a change in protein folding associated with reduced sperm motility in asthenospermic men. *Reprod. Fert.* 27, 471–480. <https://doi.org/10.1071/RD13371>.
  33. Feng, J., Zhang, J., Li, Y., Wang, J., Mo, P., and Lin, L. (2022). Upregulated expression of NOP2 predicts worse prognosis of gastric adenocarcinoma by promoting tumor growth. *Saudi J. Gastroenterol.* 28, 369–377. [https://doi.org/10.4103/sjg.sjg\\_573\\_21](https://doi.org/10.4103/sjg.sjg_573_21).
  34. Frye, M., and Watt, F.M. (2006). The RNA methyltransferase Misu (Nsun2) mediates Myc-induced proliferation and is upregulated in tumors. *Curr. Biol.* 16, 971–981. <https://doi.org/10.1016/j.cub.2006.04.027>.
  35. Li, C., Wang, S., Xing, Z., Lin, A., Liang, K., Song, J., Hu, Q., Yao, J., Chen, Z., Park, P.K., et al. (2017). A ROR1-HER3-IncRNA signalling axis modulates the Hippo-YAP pathway to regulate bone metastasis. *Nat. Cell Biol.* 19, 106–119. <https://doi.org/10.1038/ncb3464>.
  36. Yang, R., Liang, X., Wang, H., Guo, M., Shen, H., Shi, Y., Liu, Q., Sun, Y., Yang, L., and Zhan, M. (2021). The RNA methyltransferase NSUN6 suppresses pancreatic cancer development by regulating cell proliferation. *EBioMedicine* 63, 103195. <https://doi.org/10.1016/j.ebiom.2020.103195>.
  37. Liu, J., Huang, T., Chen, W., Ding, C., Zhao, T., Zhao, X., Cai, B., Zhang, Y., Li, S., Zhang, L., et al. (2022). Developmental mRNA m(5)C landscape and regulatory innovations of massive m(5)C modification of maternal mRNAs in animals. *Nat. Commun.* 13, 2484. <https://doi.org/10.1038/s41467-022-30210-0>.
  38. Selmi, T., Hussain, S., Dietmann, S., Heiß, M., Borland, K., Flad, S., Carter, J.M., Dennison, R., Huang, Y.L., Kellner, S., et al. (2021). Sequence- and structure-specific cytosine-5 mRNA methylation by NSUN6. *Nucleic Acids Res.* 49, 1006–1022. <https://doi.org/10.1093/nar/gkaa1193>.
  39. Haag, S., Warda, A.S., Kretschmer, J., Günnigmann, M.A., Hübartner, C., and Bohnsack, M.T. (2015). NSUN6 is a human RNA methyltransferase that catalyzes formation of m5C72 in specific tRNAs. *Rna* 21, 1532–1543. <https://doi.org/10.1261/rna.051524.115>.
  40. Awah, C.U., Winter, J., Mazdoom, C.M., and Ogunwobi, O.O. (2021). NSUN6, an RNA methyltransferase of 5-mC controls glioblastoma response to temozolomide (TMZ) via NELFB and RPS6KB2 interaction. *Cancer Biol. Ther.* 22, 587–597. <https://doi.org/10.1080/15384047.2021.1990631>.
  41. Liu, R.J., Long, T., Li, J., Li, H., and Wang, E.D. (2017). Structural basis for substrate binding and catalytic mechanism of a human RNA:m5C methyltransferase NSun6. *Nucleic Acids Res.* 45, 6684–6697. <https://doi.org/10.1093/nar/gkx473>.
  42. Liu, J., Huang, T., Zhang, Y., Zhao, T., Zhao, X., Chen, W., and Zhang, R. (2021). Sequence- and structure-selective mRNA m(5)C methylation by NSUN6 in animals. *Natl. Sci. Rev.* 8, nwaa273. <https://doi.org/10.1093/nsr/nwaa273>.
  43. Bex, G., Cleton-Jansen, A.M., Nollet, F., de Leeuw, W.J., van de Vijver, M., Cornelisse, C., and van Roy, F. (1995). E-cadherin is a tumour invasion suppressor gene mutated in human lobular breast cancers. *EMBO J.* 14, 6107–6115. <https://doi.org/10.1002/j.1460-2075.1995.tb00301.x>.
  44. Schaefer, M., Kapoor, U., and Jantsch, M.F. (2017). Understanding RNA modifications: the promises and technological bottlenecks of the ‘epitranscriptome’. *Open Biol.* 7, 170077. <https://doi.org/10.1098/rsob.170077>.
  45. Gu, C., Shi, X., Dai, C., Shen, F., Rocco, G., Chen, J., Huang, Z., Chen, C., He, C., Huang, T., and Chen, C. (2020). RNA m(6A) Modification in Cancers: Molecular Mechanisms and Potential Clinical Applications. *Innovation* 1, 100066. <https://doi.org/10.1016/j.xinn.2020.100066>.
  46. Huang, M., Long, J., Yao, Z., Zhao, Y., Zhao, Y., Liao, J., Lei, K., Xiao, H., Dai, Z., Peng, S., et al. (2023). METTL1-Mediated m7G tRNA Modification Promotes Lenvatinib Resistance in Hepatocellular Carcinoma. *Cancer Res.* 83, 89–102. <https://doi.org/10.1158/0008-5472.Can-22-0963>.
  47. Han, H., Yang, C., Ma, J., Zhang, S., Zheng, S., Ling, R., Sun, K., Guo, S., Huang, B., Liang, Y., et al. (2022). N(7)-methylguanosine tRNA modification promotes esophageal squamous cell carcinoma tumorigenesis via the RPTOR/ULK1/autophagy axis. *Nat. Commun.* 13, 1478. <https://doi.org/10.1038/s41467-022-29125-7>.
  48. Liu, H., Zeng, X., Ren, X., Zhang, Y., Huang, M., Tan, L., Dai, Z., Lai, J., Xie, W., Chen, Z.,

- et al. (2023). Targeting tumour-intrinsic N(7)-methylguanosine tRNA modification inhibits MDSC recruitment and improves anti-PD-1 efficacy. *Gut* 72, 1555–1567. <https://doi.org/10.1136/gutjnl-2022-327230>.
49. Dai, Z., Liu, H., Liao, J., Huang, C., Ren, X., Zhu, W., Zhu, S., Peng, B., Li, S., Lai, J., et al. (2021). N(7)-Methylguanosine tRNA modification enhances oncogenic mRNA translation and promotes intrahepatic cholangiocarcinoma progression. *Mol. Cell* 81, 3339–3355.e8. <https://doi.org/10.1016/j.molcel.2021.07.003>.
50. Wu, Y., Xie, L., Wang, M., Xiong, Q., Guo, Y., Liang, Y., Li, J., Sheng, R., Deng, P., Wang, Y., et al. (2018). Mettl3-mediated m(6)A RNA methylation regulates the fate of bone marrow mesenchymal stem cells and osteoporosis. *Nat. Commun.* 9, 4772. <https://doi.org/10.1038/s41467-018-06898-4>.
51. Chen, Z., Zhu, W., Zhu, S., Sun, K., Liao, J., Liu, H., Dai, Z., Han, H., Ren, X., Yang, Q., et al. (2021). METTL1 promotes hepatocarcinogenesis via m(7) G tRNA modification-dependent translation control. *Clin. Transl. Med.* 11, e661. <https://doi.org/10.1002/ctm2.661>.

**STAR★METHODS**

**KEY RESOURCES TABLE**

REAGENT or RESOURCE	SOURCE	IDENTIFIER
<b>Antibodies</b>		
Anti-rabbit IgG HRP-linked Antibody	Cell signaling technology	Cat# 7074S; RRID:AB_2099233
Anti-mouse IgG HRP-linked Antibody	Cell signaling technology	Cat# 7076S; RRID:AB_330924
Mouse monoclonal anti-puromycin	Millipore	Cat# MABE343; RRID:AB_2566826
Rabbit polyclonal anti- $\alpha$ -Tubulin	Proteintech	Cat# 11224-1-AP; RRID:AB_2210206
Rabbit polyclonal anti-Ki67	Abcam	Cat# ab15580; RRID:AB_443209
Rabbit polyclonal anti- Ecadherin	Proteintech	Cat# 20874-1-AP; RRID:AB_10697811
goat anti-rabbit IgG H&L DyLight® 594	Abcam	Cat# ab96885; RRID:AB_10680092
Rabbit polyclonal anti-NSUN6	Proteintech	Cat# 17240-1-AP; RRID:AB_2878367
Rabbit polyclonal anti-ELP3	Proteintech	Cat# 17016-1-AP; RRID:AB_2918048
Rabbit polyclonal anti-THUMPD1	Proteintech	Cat# 14921-1-AP; RRID:AB_2271785
Rabbit polyclonal anti-ALKBH8	Abclonal	Cat# A7142; RRID:AB_2767697
Rabbit polyclonal anti-PUS3	Proteintech	Cat# 17248-1-AP; RRID:AB_2237874
<b>Biological samples</b>		
Human ESCC tissues	Sun Yat-Sen University Cancer Center	N/A
<b>Chemicals, peptides, and recombinant proteins</b>		
Puromycin	Solarbio	Cat# P8230
Fetal bovine serum	GIBCO	Cat# A3160801
Lipofectamine 3000	Invitrogen	Cat# L3000015
Polybrene	Solarbio	Cat# H8761
Cycloheximide	MedchemExpress	Cat# HY-12320
Trizol reagent	Life technologies	Cat# 15596018
MOPS	BioFroxx	Cat# 1173GR100
MgCl <sub>2</sub>	Aladdin	Cat# M113687
NaCl	Aladdin	Cat# C111549
Triton™ X-100	Sigma	Cat# 78787
PMSF	Roche	Cat# 10837091001
<b>Critical commercial assays</b>		
Cell Counting Kit-8	Dojindo laboratories	Cat# CK04
BeyoClick EdU Cell Proliferation Kit	Beyotime	Cat# C0071S
GTVision™ III Detection System/ Mo&Rb(Including DAB)	GeneTech	Cat# GK500705
<b>Deposited data</b>		
Raw data of RNC-seq	This study	GEO: (GSE242287)
Original western blotting images	This study	Mendeley data ( <a href="https://doi.org/10.17632/3rdxrp9wj2.1">https://doi.org/10.17632/3rdxrp9wj2.1</a> )
<b>Experimental models: Cell lines</b>		
KYSE150	EK-Bioscience Biotechnology	CC-Y1705M
KYSE30	EK-Bioscience Biotechnology	CC-Y1314M
293T	ATCC	CRL-3216
ECA109	EK-Bioscience Biotechnology	CC-Y1150

(Continued on next page)

<b>Continued</b>		
REAGENT or RESOURCE	SOURCE	IDENTIFIER
HEEC	Nanjing shrbio, China	SHC6723
Experimental models: Organisms/strains		
BALB/c nude mice	Experimental Animal Center of the First Affiliated Hospital of Sun Yat-sen University	N/A
Oligonucleotides		
qPCR primers of hGAPDH-R: ACCACCCTGTTGCTGTAGCCAA	This study	N/A
qPCR primers of hGAPDH-F: GTCTCCTCTGACTTCAACAGCG	This study	N/A
qPCR primers of hCDH1-R: GAAAACAGCAAAGGGCTTGGA	This study	N/A
qPCR primers of hCDH1-F: TTAGGGCTGTGTACGTGCTG	This study	N/A
Software and algorithms		
GraphPad Prism	<a href="https://www.graphpad.com/scientific-software/prism/">https://www.graphpad.com/scientific-software/prism/</a>	N/A
ImageJ 1.8.0	<a href="https://imagej.nih.gov/ij">https://imagej.nih.gov/ij</a>	N/A
DESeq2	<a href="https://bioconductor.org/packages/release/bioc/html/DESeq2.html">https://bioconductor.org/packages/release/bioc/html/DESeq2.html</a>	N/A
GSEA	<a href="https://www.gsea-msigdb.org/gsea/index.jsp">https://www.gsea-msigdb.org/gsea/index.jsp</a>	N/A
QuPath	<a href="https://qupath.github.io/">https://qupath.github.io/</a>	N/A

## RESOURCE AVAILABILITY

### Lead contact

Requests for further information, data, and other resources can be directed to and will be fulfilled by the Lead Contact, Shuishen Zhang ([zhangshsh9@mail.sysu.edu.cn](mailto:zhangshsh9@mail.sysu.edu.cn)).

### Materials availability

This study did not generate new materials.

### Data and code availability

Raw data and processed data of RNC-seq datasets generated during this study have been deposited on GEO and are publicly available as of the date of publication. Accession numbers are listed in the [key resources table](#). Original western blotting images have been deposited at Mendeley and are publicly available as of the date of publication. The DOI is listed in the [key resources table](#). Microscopy data reported in this paper will be shared by the [lead contact](#) upon request.

This paper does not report original code.

Any additional information required to reanalyze the data reported in this paper is available from the [lead contact](#) upon request.

## EXPERIMENTAL MODEL AND STUDY PARTICIPANT DETAILS

### Patient samples

ESCC tumor tissues from 120 esophageal carcinoma patients who underwent esophagectomy between September 2002 and July 2019 were obtained from the Sun Yat-Sen University Cancer Center (Guangzhou, China). Paraffin-embedded specimens were used for immunohistochemistry (IHC) analysis. Informed consents were obtained from all patients prior to analysis. All patient-related studies were reviewed and approved by the Institutional Review Board of the hospital (B2021-131-01).

### Xenograft mouse model

BALB/c nude mice were procured from the Experimental Animal Center at the First Affiliated Hospital of Sun Yat-sen University (Guangzhou, China) and maintained under controlled conditions including a 12/12-hour light/dark cycle (lights on at 8 am), a temperature of  $23 \pm 2^\circ\text{C}$ , humidity maintained at  $55 \pm 10\%$ . The committee has established constraints on tumor growth, with the animal's original body weight

not exceeding a 10% increase and the average tumor diameter limited to 20 mm. In the subcutaneous implantation model,  $5 \times 10^6$  ESCC cells were injected into randomly grouped 6-week-old female BALB/c nude mice. The length (a) and width (b) of the tumors were measured at designated time points using calipers, and the tumor volumes (V) were computed using the formula  $V = 1/2 \times a \times b^2$ . This study adheres to the Animal Research: Reporting of *In Vivo* Experiments (ARRIVE) guidelines. The protocols involving animals were subjected to review and received approval from the Animal Care and Use Committee at the First Affiliated Hospital of Sun Yat-sen University (Approval No: 2022-005).

## METHOD DETAILS

### Data retrieval and preprocessing

The list of 115 RNA modification-related genes (RMGs) was downloaded from Modomics (<https://iimcb.genesilico.pl/modomics/>), a database of RNA modifications. Transcriptome data and corresponding clinical information for ESCC samples were sourced from the TCGA database. Samples lacking complete survival data were excluded, culminating in a refined dataset that encompassed 79 ESCC samples with comprehensive clinical attributes, which served as the foundation for subsequent analytical endeavors.

### Modeling of prognostic relevance

The role of RMGs in the prognosis of ESCC patients was determined by univariate Cox regression analysis;  $P < 0.05$  was considered significant. Risk characteristics were established by the least absolute shrinkage and selection operator (LASSO) Cox regression algorithm and multivariate Cox regression analysis. The characteristics were expressed as follows: risk score =  $(-0.8424 \times \text{expression of NSUN6}) + (-0.0986 \times \text{expression of ALKBH8}) + (-0.5032 \times \text{expression of ELP3}) + (-0.3364 \times \text{expression of PUS3}) + (-0.052 \times \text{expression of THUMP1})$ . The median risk score was used as a threshold for categorizing patients into high-risk and low-risk groups. Receiver operating characteristic curve (ROC) analysis over time was performed using the R software package "survival ROC" to assess the accuracy of the prediction of genetic characterization of cancer mortality over time. Area under the curve (AUC) was calculated to assess the accuracy of the risk prediction model. The survival analysis of different groups was estimated based on the Kaplan–Meier method using the survival package and the survminer package of R language, and log-rank test was used to determine the significance of the difference in survival rate between different groups with  $P < 0.05$  as a significance threshold.

### Construction of a predictive nomogram

Independent prognostic factors identified through multivariate Cox regression analysis with the RMS package (<https://cran.cran.r-project.org/package=RMS>) were used to develop a nomogram to predict overall survival probabilities. A calibration curve was generated to assess the disparity between the predicted probabilities from the nomogram and the actual incidence.

### Cell culture

KYSE150, KYSE30, and ECA109 cells were purchased from Shanghai EK-Bioscience Biotechnology Co., Ltd.. 293T cells were purchased from American Type Culture Collection (ATCC). All cells were cultured in DMEM (Gibco, USA) containing 10% fetal bovine serum (FBS, Gibco, USA) in a water-saturated atmosphere under 5% CO<sub>2</sub> at 37°C in an incubator (Thermo Scientific, USA).

### Knockdown or overexpression of NSUN6 in ESCC cells

Lentiviral vectors expressing pLKO.1 shRNA targeting GFP (shGFP), and NSUN6 (shNSUN6) were constructed and used for lentivirus production. The lentiviral vectors, packaging vector pCMV- $\Delta$ R8.9, and enveloped vector pCMV-VSVG were co-transfected into 293T cells using Lipofectamine 3000 reagent (Invitrogen, USA). After 48 hours of transfection, the packaged viruses were harvested and utilized to infect ESCC cells (KYSE150 and KYSE30) with the addition of 10  $\mu$ g/ml Polybrene (Solarbio, China). To select the infected cells, 2.5  $\mu$ g/ml puromycin (Solarbio, China) was administered for 48 hours. For overexpression of NSUN6 or E-cadherin, the full-length ORF of human NSUN6 gene or human CDH1 gene was inserted into pCDH plasmid and used for lentivirus production.

### Western blotting

The proteins to be tested were first separated by SDS-PAGE gel electrophoresis, and then the proteins were migrated onto a PVDF membrane. Next, the membrane is blocked by TBST containing 3% BSA. Subsequently, the membrane was incubated in the antibody solution to bind the primary antibody to the target protein. After washing, the secondary antibody is bound to the primary antibody complex and the protein bands are detected using a chemiluminescent imaging device.

### Colony-formation, cell proliferation assays

For the cellular growth evaluation, a total of 1,500 ESCC cells were seeded into 96-well plates. The assessment of cellular proliferation took place over the subsequent five days from the time of seeding, employing the Cell Counting Kit-8 (Dojindo, Japan) following the manufacturer's instructions. EdU cell proliferation assay was performed using the BeyoClick EdU Cell Proliferation Kit (Beyotime, China). To identify cell proliferation, 5-ethynyl-2'-deoxyuridine (EdU) was added into the culture medium, allowing it to be absorbed and marking newly synthesized DNA. Following this phase, EdU is tagged through the application of a click chemistry technique, leading to the visualization of fluorescence signals.

that serve to assess cell proliferation activity. As for the colony formation analysis, 500 cells were evenly distributed into 6-well plates and subsequently cultured for 10 days. Due to excessive inhibition of clone formation caused by overexpression, we utilized twice the number of cells in Figure 5C. The quantification of colonies stained with 0.5% crystal violet was executed utilizing ImageJ (version 1.53n).

### Wound healing

$1 \times 10^6$  cells were seeded into the well of 6-well culture plates containing 2 ml culture medium with FBS and cultured until confluent. A pipette tip was used to make a straight scratch in each well. Then the cells were incubated with DMEM (Gibco, USA) without FBS. The width of the scratch at 0 hour and 48 hours were recorded after scratching under a microscope.

### Transwell invasion

For invasion assay,  $5 \times 10^4$  cells in 200  $\mu$ l medium with 2% FBS were added into the upper chamber of a transwell insert (pore size, 8  $\mu$ m; Corning Falcon, pre-coated with 100  $\mu$ l matrigel) and placed on a receiver well containing 600  $\mu$ l medium supplemented with 20% FBS. After 40 hours, the chambers were collected and stained with 0.5% crystal violet. The migrated cells were then counted.

### Immunohistochemistry (IHC) staining

Immunohistochemical analysis was conducted following the guidelines outlined in the kit instructions (GeneTech, China). The primary antibodies used were as follows: Anti-Ki67 (1:1000 diluted, Proteintech); Anti-ELP3 (1:1000 diluted, Proteintech); Anti-NSUN6 (1:500 diluted, Proteintech); Anti-THUMP1 (1:500 diluted, Proteintech); Anti-ALKBH8 (1:500 diluted, Abclonal); Anti-PUS3 (1:500 diluted, Proteintech). Evaluation of IHC staining was carried out using QuPath (v0.2.3) and quantified in terms of H-score.

### RNA mass spectrometry analysis

tRNAs were first purified from total RNAs by Urea-PAGE electrophoresis and size selection. Then total RNAs and the purified tRNAs were digested into single nucleosides, which were then analyzed by liquid chromatography-coupled mass spectrometry (LC-MS) using the Agilent 6460 QQQ mass spectrometer with an Agilent 1260 HPLC system. The levels of m<sup>5</sup>C RNA modifications in different samples were calculated as ratio of m<sup>5</sup>C RNA modification normalized peak area to the sum of the normalized peak area of all detected nucleosides in total RNAs or tRNAs.

### Ribosome-nascent chain complex-bound mRNA sequencing (RNC-seq)

In brief, cells were exposed to a concentration of 100  $\mu$ g/ml cycloheximide for 3 minutes, followed by treatment with a cell lysis buffer containing 1% Triton X-100, 200 mM KCl, 15 mM MgCl<sub>2</sub>, 20 mM HEPES-KOH (pH 7.4), 100  $\mu$ g/ml cycloheximide, and 2 mM dithiothreitol on ice for 30 minutes. Subsequently, the cellular lysate was subjected to centrifugation at  $16,200 \times g$  for 10 minutes at 4°C. The supernatant was then delicately layered onto 11 ml of sucrose buffer (30% sucrose in RB buffer). Through an ultracentrifugation step at  $185,000 \times g$  for 3 hours at 4°C, the mRNA bound to polyribosomes was selectively pelleted. The obtained polyribosome-bound mRNA was subsequently purified using TRIzol reagent (Invitrogen, USA). To establish cDNA libraries, sequencing was conducted utilizing the BGISEQ-500 platform (BGI, Shenzhen, China). The translation efficiency (TE) of each gene was determined by comparing its transcript per million (TPM) value in the RNC-mRNA to that in the input-RNA. Genes with foldchange of TEs (shGFP/shNSUN6) > 2 were defined as down-regulated genes.

### RNA isolation and qRT-PCR

Total RNAs were isolated using Trizol reagent (Invitrogen, USA) following the manufacturer's instructions. 2  $\mu$ g RNA was used to perform reverse transcription by HiScript III RT SuperMix for qPCR Kit (Vazyme, China). Next, the cDNAs were 1:10 diluted followed by qRT-PCR using TB Green™ Premix Ex Taq™ II (Takara, Japan) in StepOnePlus™ real-time PCR system (Thermo Scientific, USA). GAPDH was used as an internal control.

### Immunofluorescence

The tissues were processed and incubated with primary antibodies (Anti-Ecadherin, proteintech, 1:300 dilution) following the IHC protocol, and the blocking buffer containing 5% normal donkey serum, 1% BSA and 0.2% Triton X-100 was used in the blocking step. Then the slides were incubated with secondary antibody (goat anti-rabbit IgG H&L DyLight® 594, Abcam, 1:300 dilution) at room temperature for 50 minutes, followed by treatment with 4, 6-diamidino-2-phenylindole at room temperature for 5 minutes. The fluorescence signal was then detected and imaged under a microscope (ZEISS, Germany).

### Gene pathway enrichment and depmap analysis

Gene Ontology and Pathway Analysis were employed to perform the enrichment analysis of pathways. The gene pathway analysis of differentially translated mRNAs identified from polyribosomal sequencing data was executed using the ToppFun module within the ToppGene Suite. (<https://toppgene.cchmc.org/enrichment.jsp>). The gene sets for GSEA were downloaded from GSEA portal (<https://www.gsea-msigdb.org/gsea/index.jsp>), and the translation matrix was analyzed using GSEA version 4.1 portal. The expression and perturbation effects of different RMGs in ESCC were evaluated by using the data in Depmap (<https://depmap.org/portal/>).

### QUANTIFICATION AND STATISTICAL ANALYSIS

The student's t-test (two-tailed) was employed to assess differences between two groups. One-way ANOVA with Dunnett's multiple comparison test was employed to assess differences between three or more groups. Univariate and multivariate Cox regression analyses were utilized to identify independent prognostic factors for patients with ESCC. The Kaplan–Meier method and log-rank test were applied to compare overall survival (OS) differences among different groups. Data analysis was conducted using GraphPad Prism 8.3 (GraphPad, San Diego, CA, USA) or SPSS v23.0 (IBM Corp., Armonk, NY, USA). All statistical tests were two-sided, and a  $P$  value  $< 0.05$  was considered statistically significant. The statistical details were indicated in the figure legends. ns =  $P > 0.05$ , \* =  $P < 0.05$ , \*\* =  $P < 0.01$ , \*\*\* =  $P < 0.001$ .

### ADDITIONAL RESOURCES

ESCC tumor tissues from 120 esophageal carcinoma patients were obtained from the Sun Yat-Sen University Cancer Center. All patient-related studies were reviewed and approved by the Institutional Review Board of the hospital (approval no. B2021-131-01).